Analysis of GaSb and AlSb reconstructions on GaSb(111) *A*- and *B*-oriented surfaces by azimuthal-scan reflection high-energy electron diffraction

Andre Proessdorf,* Frank Grosse, Wolfgang Braun, Ferhat Katmis, and Henning Riechert
Paul-Drude Institut für Festkörperelektronik, Hausvogteiplatz 5–7, D-10117 Berlin, Germany

Oleksandr Romanyuk
Institute of Physics, Academy of Sciences of the Czech Republic, Cukrovarnicka 10, 162 00 Prague, Czech Republic
(Received 3 November 2010; revised manuscript received 8 February 2011; published 21 April 2011)

The symmetry and existence ranges of GaSb and AlSb (111) *A* and *B* surface reconstructions are investigated using azimuthal-scan reflection high-energy electron diffraction (ARHEED) in a molecular-beam-epitaxy (MBE) environment. ARHEED patterns of all reconstructions within the accessible MBE group V flux-substrate temperature parameter field are presented and analyzed. The transition borders are mapped out as a reference for future growth experiments. The experimental results are interpreted on the basis of general construction principles for (111) surfaces of III-V semiconductors. ARHEED allows the complete determination of the two-dimensional in-plane reciprocal lattice in a single, continuous measurement. This allows the unambiguous identification of the reconstructions on (111) surfaces where the intrinsic symmetry is masked by the 120° domain structure and possible disorder.

DOI: 10.1103/PhysRevB.83.155317 PACS number(s): 68.35.B−, 68.35.Md, 68.47.Fg

I. INTRODUCTION

Reflection high-energy electron diffraction (RHEED) is used routinely for *in situ* growth control in molecular-beam epitaxy (MBE). Instead of scanning only along planes normal to the surface, it was shown by Ino[1] and later by Braun *et al.*[2,3] and Ichimiya *et al.*[4] that RHEED offers significantly more information when the in-plane direction along the incident beam is included. This direction is accessible through azimuthal sample rotation. Compared to the standard use of RHEED, where symmetries along the main crystallographic directions are recorded in a surface normal plane, azimuthal-scan reflection high-energy electron diffraction (ARHEED) has the advantage of mapping the entire two-dimensional (2D) in-plane symmetry of the surface. It is therefore especially useful when the formation of rotated surface domains, e.g., due to twinning of the (111)-oriented layers or the formation of antiphase domains in (001)-oriented layers, reconstruction domains, or disorder complicate an unambiguous identification of the surface reconstruction.

The surfaces of III-V compound semiconductors have been studied by various experimental methods such as x-ray diffraction (XRD),[5] scanning tunneling microscopy (STM),[6,7] photoemission spectroscopy (PES),[8–10] transmission electron diffraction (TED),[11] and low-energy electron diffraction (LEED). The majority of these efforts focused on the analysis of surface structures on (001) substrates,[12–17] the reconstruction phase diagrams,[18,19] and the understanding of their growth kinetics.[20] The group III-Sb(111) surfaces have not attracted that much attention so far, although the group III-Sb based semiconductors are suitable materials for device applications in near- and mid-infrared optical devices and in high-speed electronics. Their high electron mobility offers the potential for integrated magnetic sensors[21] and quantum cascade lasers.[22] Heterostructures on GaAs,[23] InP,[24] and GaSb (Refs. 25 and 26) substrates have been explored for device applications.

The (111) surface orientation has been investigated for the growth of various material combinations and shown to offer advantageous properties. For instance, the formation of antiphase domains is avoided in III-V growth on Si,[27,28] rare-earth oxides coherently grow on Si(111),[29] and the majority of nanowires typically grow along [111] on (111)-oriented substrates.[30] Since nanoscale devices may include only a few atomic layers, the influence of surface structures on the functional interfaces and ultrathin layers that are formed by crystal growth becomes crucial and needs to be investigated in advance.

In earlier works, the GaSb(111)*A* (2×2) reconstruction was prepared by argon-ion bombardment followed by sequential cycles of annealing.[31–33] This surface structure was later investigated by x-ray diffraction[34,35] and photoemission techniques.[36] The (2×2) reconstruction was also prepared by interdiffusion-assisted MBE of GaSb on Sb(111) surfaces.[37] In this scheme, a Ga flux was introduced to Sb(111) substrates from effusion cells at elevated temperatures, with the Sb diffusing in from the substrate. Such experimental conditions correspond to an Sb-poor regime. At the opposite end, Sb-rich conditions can be achieved by supplying Sb to the surface. We have analyzed the stabilization of the $(2\sqrt{3} \times 2\sqrt{3})$ reconstruction on the GaSb(111)*A* surface by configurational entropy, as observed experimentally.[38]

MBE was used for GaSb homoepitaxial growth on on-axis GaSb(001) and (111)*B* surfaces.[39] The GaSb(111)*A* and *B* surfaces were investigated by Dura *et al.*[40,41] They investigated the surface structure by RHEED and observed the periodicity along the $[\bar{1}10]$ and $[\bar{1}\bar{1}2]$ directions. The following surface symmetries were reported: GaSb(111)*A*: (2×2), (5×2), and (2×6); GaSb(111)*B*: (8×2) and (3×3). To the best of our knowledge, AlSb(111) reconstructions have not been analyzed so far. The likely reason is a high reactivity of AlSb at elevated pressures. Bulk AlSb substrates are not available, since the material rapidly oxidizes in air.[42]

The paper is organized as follows. The surface preparation technique, the Sb flux, and substrate temperature calibration procedures, as well as the buffer layer growth, are explained in Sec. II. A description of the ARHEED technique follows. The various resulting reconstructions of GaSb and AlSb on the (111)*A* and (111)*B* surface, which are achieved by variation of the Sb_4 flux and substrate temperature, are presented in Sec. III. Possible configurational arrangements on the surface are discussed on the basis of the observed surface reconstructions. Finally, the main results are summarized in Sec. IV.

II. EXPERIMENTAL DETAILS

GaSb and AlSb/GaSb(111)*A* and *B* surfaces are prepared in the Createc PHARAO MBE chamber[43] at BESSY II under ultrahigh-vacuum (UHV) conditions. The pressure in the chamber during the experiments was below 8×10^{-10} mbar. Undoped 1-mm-thick 2-in. GaSb (111)*A* and *B* wafers from Wafer Technology LTD were used, cut into quarters and loaded into the load-lock chamber. An intermediate preparation chamber serves to further clean the samples in a second outgassing step. Deposition is performed using an Al cold lip effusion cell, a Ga hot lip effusion cell, and a (noncracking) Sb hot lip effusion cell. Control of the growth as well as the surface scattering experiments were done using RHEED. The RHEED gun was operated at an electron energy of 20 keV and a filament current of 2 A. A standard phosphorus screen is imaged by a charge-coupled device (CCD) camera with a resolution of 640×480 pixels^2 and 12-bit dynamic range. The resulting images are processed by a digital image acquisition RHEED system.[44]

A. Substrate temperature and cell calibration

Special attention needs to be given to the calibration of the Sb_4 fluxes and the substrate temperature to ensure reproducible surface preparation and epitaxial growth. The substrate is heated by a resistive wire heater a few mm away and the substrate temperature is measured by a noncontact thermocouple. The estimated intrinsic accuracy of the temperature measurement is ±50 K.

To improve this value, three calibration points are introduced: the Sb crystallization temperature at 222 °C, Sb desorption at 255 °C, and oxide desorption at 450 °C. These calibration points vary from sample to sample with a reproducibility of ± 5 K.

To calibrate the Sb_4 flux, Sb is deposited on Si for 60 min at room temperature with six different Sb_4 effusion cell temperatures. The thicknesses and densities of the grown layers are then determined by x-ray reflectivity. Each layer thickness is verified by scanning electron microscopy (SEM) on the cleaved edge. The variation of the Sb growth rate with effusion cell temperature is determined by assuming a Sb sticking coefficient of one at room temperature.[45] The experimental data points and the Arrhenius fit of these values are given in Fig. 1. The two calibration curves in Fig. 1 are determined five months apart and the shift of the curves is caused by the depletion of the Sb_4 effusion cell. The data set 1 calibration is used in this work.

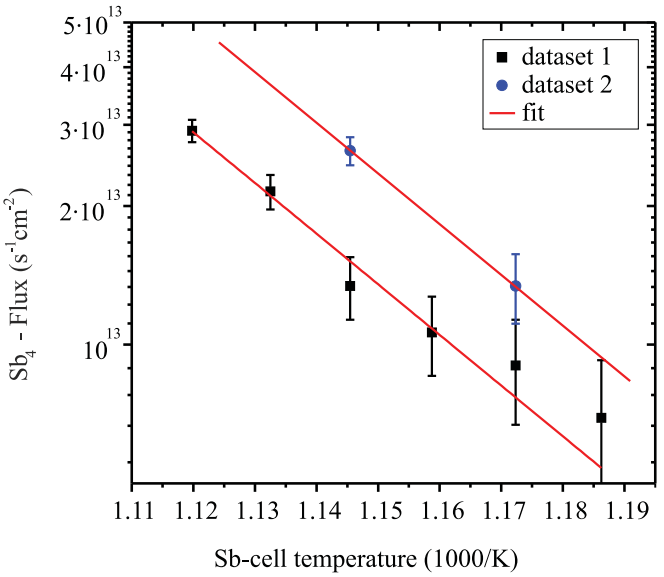

FIG. 1. (Color online) Sb_4 flux in number of Sb_4 molecules per time and area vs effusion cell temperature (for details, see the text). The data sets 1 and 2 are measured 5 months apart.

B. Oxide desorption and surface smoothing

To prepare a smooth surface, the native oxide is desorbed and a smooth buffer layer is grown on the GaSb(111)*A* and *B* surface. At first, the substrate is loaded into the load-lock chamber and outgassed for 10 min at 150 °C at a pressure of 6×10^{-8} mbar. Then, the sample is transferred to the preparation chamber and heated for 30 min at 350 °C at a pressure of 6×10^{-10} mbar. Next, the sample is introduced into the growth chamber, at which stage RHEED produces the pattern shown in Fig. 2(a).

Maintaining a constant Sb_4 flux of 1.4×10^{13} Sb_4 molecules s^{-1} cm^{-2}, the sample is heated from room temperature to 400 °C at a rate of 0.2 °C/s while being monitored by RHEED. The following patterns are distinguished. Up to 255 °C substrate temperature, a polycrystalline Sb layer is formed, indicated by rings in the diffraction pattern [Fig. 2(b)]. With increasing substrate temperature, Sb desorbs from the surface and the amorphous native oxide appears [Fig. 2(c)]. Increasing the substrate temperature further at a

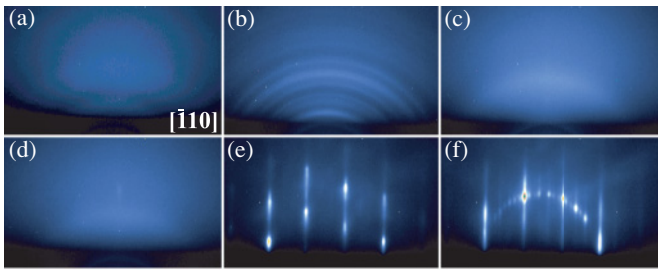

FIG. 2. (Color online) RHEED patterns recorded during buffer layer growth on GaSb(111)*B*. (a) After loading into the growth chamber at room temperature, (b) polycrystalline pattern at 170 °C, (c) amorphous pattern at 400 °C, (d) beginning oxide desorption at 450 °C, (e) after annealing for 20 min at 470 °C, and (f) after buffer layer growth at 400 °C.

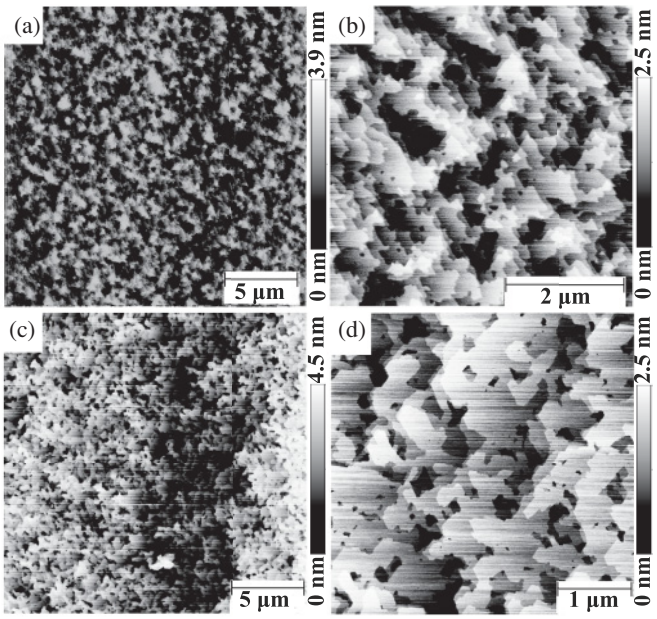

FIG. 3. AFM of a GaSb(111)*A* surface: (a) $20 \times 20\ \mu m^2$ with 0.38 nm rms roughness, (b) $5 \times 5\ \mu m^2$ with 0.32 nm rms roughness; GaSb(111)*B* surface: (c) $20 \times 20\ \mu m^2$ with 0.41 nm rms roughness, and (d) $4 \times 4\ \mu m^2$ with a rms roughness of 0.55 nm.

rate of 0.1 °C/s, the RHEED pattern reveals the first weak transmission spots at 450 °C, indicating the onset of oxide desorption [Fig. 2(d)]. After reaching 470 °C, the surface is annealed for 20 min and a reflection RHEED pattern with reduced background intensity develops [Fig. 2(e)]. To prepare buffer layer growth, the substrate temperature is finally decreased to 330 °C with a 1 K/s temperature ramp. The Ga and Sb_4 fluxes are adjusted to grow 1 monolayer (ML) per 30 s with a V/III ratio of approximately 5. After opening the Ga shutter, the substrate temperature is slowly increased by 0.1 °C/s to 400 °C, after which the Ga shutter is closed again. Finally, an annealing step of 30 min at 440 °C under constant Sb_4 flux further smoothes the grown buffer layer. The resulting surface produces the typical 2D reflections in a RHEED pattern with low background [Fig. 2(f)].

The smooth surface with large atomically flat terraces is confirmed by atomic force microscopy (AFM) images as shown in Fig. 3 for the GaSb(111)*A* and *B* surfaces. Ambient AFM measurements on the AlSb surfaces cannot be carried out since AlSb quickly oxidizes under atmospheric conditions.[42]

C. ARHEED

To obtain a two-dimensional (2D) in-plane reciprocal space map from a surface, it is necessary to take sequential images while continuously rotating the substrate at constant speed. The ARHEED technique is explained in detail elsewhere.[1–3,46,47] As a demonstration of the resolution of the method, the construction of a narrow sector of an azimuthal scan is shown in Fig. 4. The complete data for this sample are shown in Fig. 6(a).

The RHEED patterns shown in Figs. 4(a)–4(l) are equidistant snapshots from a continuous sequence. Each pattern is measured with an azimuthal separation of 0.1° so that the

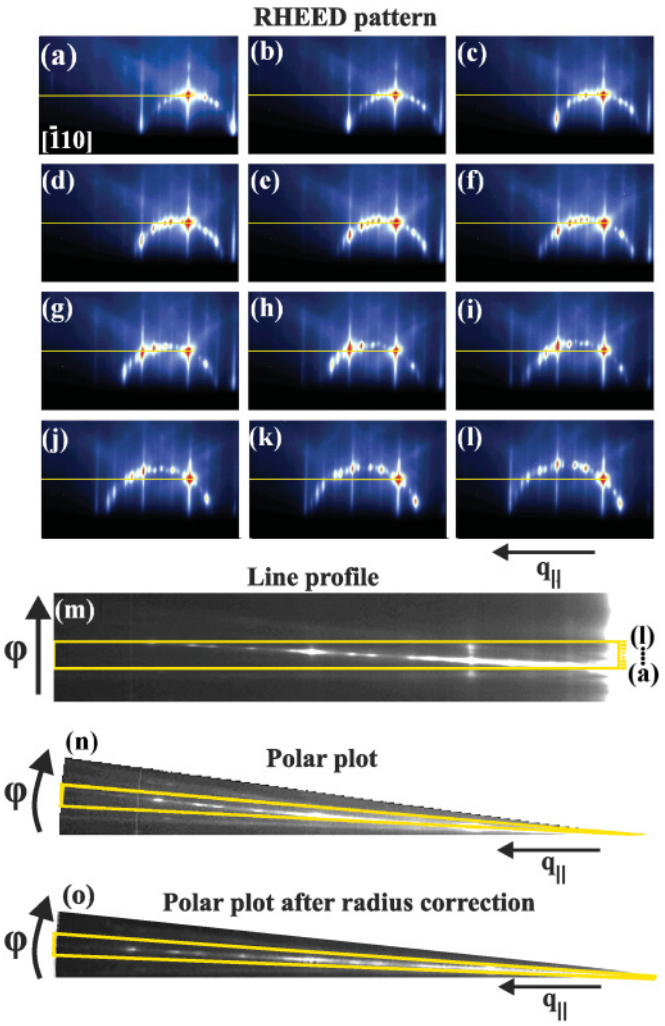

FIG. 4. (Color online) Example of an azimuthal RHEED scan measured on a GaSb(111)*B* surface. The RHEED patterns in (a)–(l) are extracted from a movie containing the diffraction pattern during continuous rotation of the sample around its surface normal. Image (m) shows the intensity along the line in (a)–(l) with time or angle direction pointing upward. In (n), the data are shown in the processed polar plot, representing a section of reciprocal space parallel to the surface at the position of the line in (a)–(l). φ is an azimuthal angle and $\vec{q}_{||}$ is a momentum transfer vector parallel to the surface. (o) shows the final result with an additional correction for the radius of the Ewald sphere to straighten the rows of reflections.

12 images of Figs. 4(a)–4(l) span 1.2° of azimuthal angle. As the sample rotates, the Laue circle crosses the line at the height of the specular spot, tracing the entire row of reflections along the high-symmetry azimuth, as demonstrated in Figs. 4(a)–4(l). The intensity along the line in Figs. 4(a)–4(l) is plotted as a function of recording time during steady-state rotation in the highlighted box in Fig. 4(m) and as function of the corresponding azimuthal angle in polar coordinates in Fig. 4(n). Finally, after bending the lines according to the radius of the Ewald sphere in Fig. 4(o), the straight line of reflections in the radial direction is obtained.

For each GaSb and AlSb(111) surface, we have measured several ARHEED patterns. The sampled azimuthal rotation

angle range varied from 70° to 150°. In the corresponding polar plots, the measured sector is shifted sideways from the rest of the pattern. To reconstruct the full 360° pattern, copies of the measured patterns are rotated according to the surface unit-cell symmetry. All observed reconstructions obey the threefold rotation symmetry of the substrate. Stationary RHEED patterns along the $[\bar{1}\bar{1}2]$ and $[\bar{1}10]$ incident directions are included for each reconstruction as well.

III. RESULTS AND DISCUSSION

In the present section, the different observed steady-state surface reconstructions of GaSb and AlSb/GaSb(111) surfaces with *A* and *B* orientation as a function of Sb_4 flux and substrate temperature are presented. The border lines of the surface reconstruction transition are determined and given in reconstruction phase diagrams.

A. GaSb(111)*A* and *B*

For the GaSb(111)*A* surface, two reconstructions can be identified, which are summarized in the reconstruction phase diagram of Fig. 5: a low-temperature (12 × 1) (Fig. 6) and a high-temperature ($2\sqrt{3} \times 2\sqrt{3}$) reconstruction (Fig. 7). The low-temperature reconstruction is stable from room temperature up to 300 °C without Sb flux. The reconstruction phase transition occurs between 300 and 340 ° C depending on the Sb_4 flux. We find that all the observed phase boundaries do not significantly shift whether we measure during heating or cooling. Such a shift could be due to floating Sb on the surface that modifies the surface reconstructions and is then desorbed at higher surface temperatures. Such a hysteresis of surface reconstructions is reported on InAs(001) (Refs. 48 and 49) and GaAs(001) (Ref. 50) surfaces and was explained due to the miscut of the substrate and the Sb_4 flux.

The previously reported GaSb(111)*A* (2 × 2) reconstruction[5] is not observed under Sb-rich conditions. However, a clear (2 × 2) diffraction pattern is measured under Ga-rich

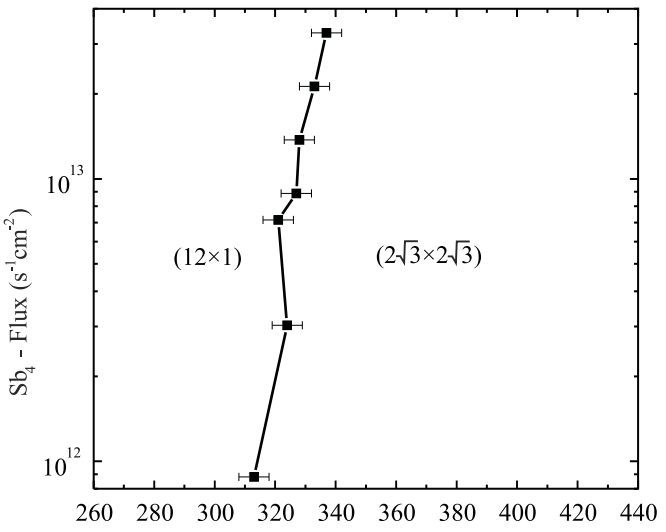

FIG. 5. Surface reconstruction phase-transition diagram for the GaSb(111)*A* surface with Sb_4 flux plotted vs substrate temperature measured by a thermocouple.

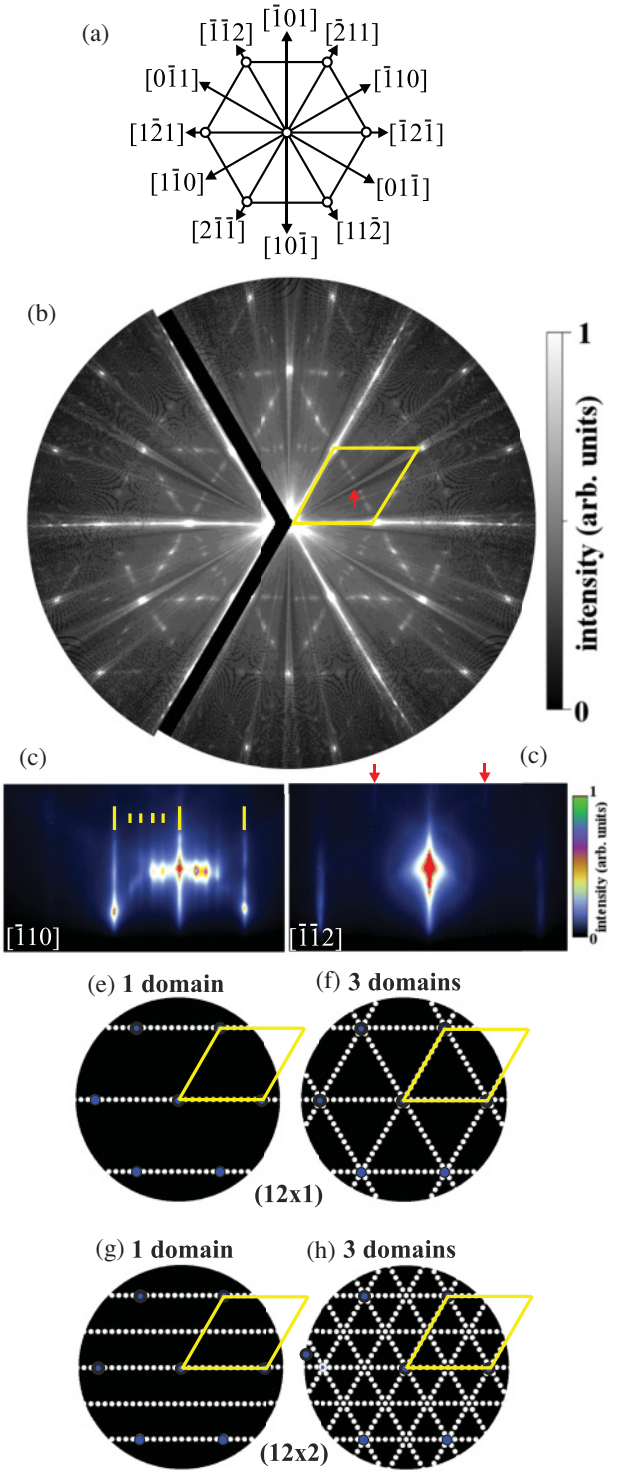

FIG. 6. (Color online) (a) The crystallographic directions of the (111) surface. The corners of the (1 × 1) unit cells in reciprocal space are indicated by circles. (b) RHEED azimuthal scan of the GaSb(111)*A* (12 × 1) reconstruction at 300 °C substrate temperature. The rhombus marks the (1 × 1) surface unit cell and the arrow points to the apparent 2 × periodicity along the $[\bar{1}\bar{1}2]$ incident direction. RHEED patterns are displayed with the electron beam along (c) $[\bar{1}10]$ and (d) $[\bar{1}\bar{1}2]$ incident directions. Diffraction symmetry of (e) (12 × 1), (f) (12 × 1) with rotated domains, (g) (12 × 2), and (h) (12 × 2) with rotated domains.

conditions achieved by opening the Ga shutter with a Ga-to-Sb flux ratio of approximately 1. The reported (2×2) reconstruction may be stable when prepared by sputtering without Sb pressure, possibly leading to an Sb-deficient surface. On the other hand, an Sb background pressure in our chamber may hinder the formation of the (2×2) reconstruction.

To analyze the full symmetry of the surface, ARHEED scans are measured for each surface reconstruction. Figure 6(a) shows the in-plane directions for the scans in this paper. The ARHEED pattern of the (12×1) reconstruction is given in Fig. 6(b). In Fig. 6(c), the positions of the four fractional-order streaks along the $[\bar{1}10]$ incident direction are marked by short lines. The long lines mark the integer-order diffraction rod positions. Dura *et al.* reported a (5×2) reconstruction in the same range of substrate temperatures and Sb fluxes.[40,41] We find that the fractional-order rods lie on a $12\times$ grid. Two distances are present in Fig. 6(d): $d_1 = 1/4$ is the distance between the integer-order rod and its neighboring fractional-order rod, and $d_2 = 1/6$ is the distance between the fractional-order rods themselves. Thus, the positions of the fractional-order rods are $(3h/12, 0)$, $(5h/12, 0)$, $(7h/12, 0)$, and $(9h/12, 0)$, where h is an integer number. The relative coordinates of these positions do not depend on substrate temperature or Sb_4 flux. The $(1h/12, 0)$, $(2h/12, 0)$, $(4h/12, 0)$, $(8h/12, 0)$, $(10h/12, 0)$, and $(11h/12, 0)$ streaks are smeared out in the diffraction pattern. The intensity of these streaks could be suppressed due to one-dimensional disorder along the surface similar to the GaAs(001) $\beta 2(2 \times 4)$ and GaSb(001) (4×3) reconstructions,[51] but most probably due to the structure itself.

Nevertheless, after a remeasuring of the diffraction pattern with a digital high-resolution RHEED camera system (1392×1024 pixels^2), all $12\times$ reflections are found. The RHEED patterns for both low and high resolution are included in the supplemental material for this paper.[52]

A weak $2\times$ periodicity is present in Fig. 6(d). This is not due to an intrinsic $(1/2, 1/2)$ peak, but is a projection of the $12\times$ periodicity along the $[\bar{1}10]$ incidence direction due to the threefold-rotated domain structure. The origin of this apparent $2\times$ periodicity is labeled with an arrow in Figs. 6(b) and 6(d). This conclusion can be derived from the complete symmetry of the reciprocal lattice obtained in the measurement. To construct the superposition, the (12×1) and (12×2) patterns are simulated with and without rotated domains using the software package LEEDPad.[53] The results are shown in Figs. 6(e)–6(h). The origin of the $2\times$ periodicity is the rotated $12\times$ azimuth of the (12×1) reconstruction. A (12×2) reconstruction with the correspondingly rotated diffraction pattern would result in a $4\times$ periodicity along the $[\bar{1}10]$ incident direction.

The low background level in the RHEED measurement of the $(2\sqrt{3} \times 2\sqrt{3})$ reconstruction in Fig. 7 together with the bright and well-defined Laue circle spots on the RHEED pattern are characteristic of a smooth surface, while the higher background level of the (12×1) reconstruction (Fig. 6) indicates a higher level of disorder on the surface. In addition, a bright fractional-order rod is visible at the $(1/2, 1/2)$ position in the RHEED pattern along the $[\bar{1}\bar{1}2]$ incident direction [Fig. 7(c)], which is caused by an overlay of $(2\sqrt{3}\times 2\sqrt{3})$ and (2×2) reconstruction patterns. Our analysis of the thermodynamic equilibrium behavior of the GaSb(111)*A* surface

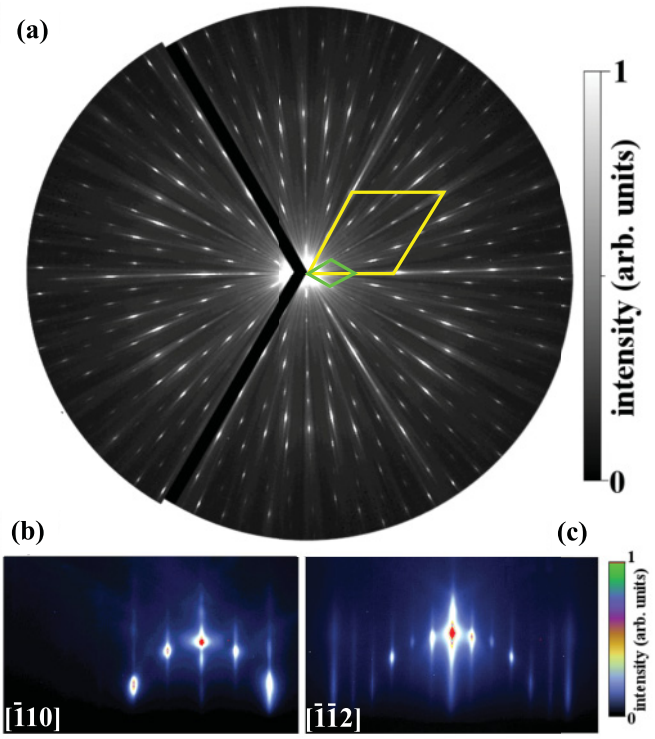

FIG. 7. (Color online) (a) RHEED azimuthal scan of the GaSb(111)*A* $(2\sqrt{3} \times 2\sqrt{3}) + (2 \times 2)$ reconstruction at 400 °C substrate temperature. The big rhombus corresponds to the (1×1) and the small rhombus to the $(2\sqrt{3} \times 2\sqrt{3})$ unit cell. RHEED patterns are along (b) $[\bar{1}10]$ and (c) $[\bar{1}\bar{1}2]$ incident directions.

on the basis of density-functional calculations has shown that the observed RHEED pattern originates from various $(2\sqrt{3} \times 2\sqrt{3})$ reconstructions, which are stabilized by configurational entropy.[38] At elevated temperatures they coexist in equilibrium with the low-energy (2×2) reconstruction, and their concentration ratio can be influenced by the substrate temperature. The coexistence of (2×2) and $(2\sqrt{3} \times 2\sqrt{3})$ domains was observed also by Nishizawa *et al.*[54] by STM on InSb(111)*A* surfaces.

At 480 °C, the RHEED pattern changes abruptly from the $(2\sqrt{3} \times 2\sqrt{3})$ to a diffuse (1×1) symmetry. In the temperature range $T_{sub} > 480$ °C, AFM measurements show a very rough surface with hillocks and droplet formation independent of the Sb_4 flux. However, at a lower substrate temperature ($T_{sub} < 480$ °C), the surface is Sb-rich arising from the remaining Sb background pressure of the growth chamber. Therefore, the surface is stabilized by Sb and the resulting surface structures are the (12×1) and $(2\sqrt{3} \times 2\sqrt{3})$ reconstructions. The reported (2×6) reconstruction[40,41] is reinterpreted due to our ARHEED measurement as a $(2\sqrt{3} \times 2\sqrt{3})$ reconstruction. The corresponding $(2\sqrt{3} \times 2\sqrt{3})$ unit cell is labeled with a small rhombus in Fig. 7(a).

The GaSb(111)*B* surface displays an (8×1) diffraction pattern after the oxide desorption process. It is stable within the entire Sb_4 flux and substrate temperature range investigated in this work. Short marker lines indicate the fractional-order rod positions measured along the $[\bar{1}10]$ incident direction of

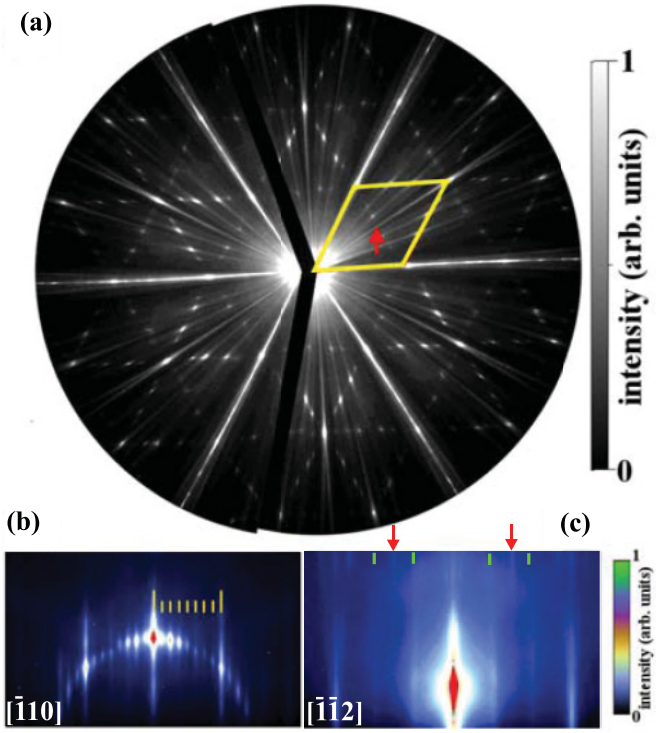

FIG. 8. (Color online) (a) RHEED azimuthal scan of the GaSb(111)*B* surface with an (8 × 1) reconstruction cooled down to room temperature. The Sb flux was closed at 300 °C substrate temperature during cooling. The rhombus corresponds to the (1 × 1) surface unit cell and the arrow points to the apparent 2× periodicity in the [$\bar{1}\bar{1}$2] direction. RHEED patterns are along (b) [$\bar{1}$10] and (c) [$\bar{1}\bar{1}$2] incident directions.

the (8 × 1) reconstruction in Fig. 8(b). Within measurement accuracy, all fractional-order rods are on exact 8 × positions. The measured distances of all fractional-order rods are $d_1 = 1/8$, and the distance does not vary with Sb_4 flux or substrate temperature.

Similar to the GaSb(111)*A* (12 × 1) reconstruction, a 2 × periodicity along the [$\bar{1}\bar{1}$2] incident direction is observed for the GaSb(111)*B* (8 × 1) under Sb-rich conditions. The position is marked by an arrow in Fig. 8(a). In addition, we observe an intensity variation in the fractional-order rods of the (8 × 1) reconstruction. The RHEED pattern along the [$\bar{1}$10] [Fig. 8(b)] incident direction shows high intensity in the (3*h*/8,0) and (5*h*/8,0) fractional-order rods, marked by short lines. Along the [$\bar{1}\bar{1}$2] incident direction, several faint reflections are observed. They are highlighted with short lines in Fig. 8(c).

Dura[40,41] and Feidenhans'l[5] report a (3 × 3) reconstruction for GaSb(111)*B* surfaces. In our experiments, we did not observe a static (3 × 3) reconstruction under Sb-rich conditions. This reconstruction only appears with an open Ga shutter during growth. Under such Ga-rich conditions, the (8 × 1) structure transforms to (3 × 3) reconstruction. The 8 × pattern along the [$\bar{1}$10] incident direction disappears and the 3 × periodicity remains with a shift of the (3*h*/8,0) and (5*h*/8,0) fractional-order rods along the [$\bar{1}$10] incident direction to the corresponding exact positions of the ordered (3 × 3) reconstruction. The intensities of the weak 3 × reflections along the [$\bar{1}\bar{1}$2] incident direction increase without shifting their positions.

B. AlSb(111)*A* and *B*

AlSb has been demonstrated to be an efficient buffer layer for heteroepitaxial growth on Si(001) (Refs. 55 and 56) or GaAs(001).[57] The shorter diffusion length of Al atoms compared to Ga seems to help in confining a larger number of relaxation-related defects at the heterointerface. To investigate the surface reconstructions of the AlSb(111) *A* and *B* surfaces, we have grown AlSb layers on GaSb(111) by MBE. Due to the rapid oxidation of AlSb in air, the reconstruction can only be investigated *in situ* under ultrahigh-vacuum conditions.

In earlier works, lattice-mismatch-related strain was studied with respect to its possible effects on the surface reconstructions by density-functional theory on InAs(001).[58] No significant differences in the reconstructions were found, although the stability region shifted in terms of flux and temperature.[58] We therefore neglect possible strain effects due to AlSb/GaSb heteroepitaxial growth, since there is only a small lattice mismatch of 0.7%.[59] The AlSb layer thickness used in this study is varied between 20 and 60 nm. For any of these values, identical surface reconstructions are observed. There is a tendency of Ga segregating into the overgrown layer on substrates such as GaAs, GaP, and GaSb.[60] Quantitatively, it was shown that the Ga surface concentration is below 1% after the deposition of 10 ML AlAs on GaAs or AlSb and InAs on GaSb, respectively.[61–64] We therefore neglect segregation effects in the present study.

In the reconstruction phase diagram of AlSb(111)*A*, four reconstructions are present (Fig. 9). Two ($2\sqrt{3} \times 2\sqrt{3}$) reconstructions exist, one below 330 °C (Fig. 10) and one above 380 °C (Fig. 13). In addition, a (7 × 1) (Fig. 11) and a diffuse (2 × 1) (Fig. 12) reconstruction are observed. The existence ranges of the different reconstructions depend on the Sb_4 flux and the substrate temperature.

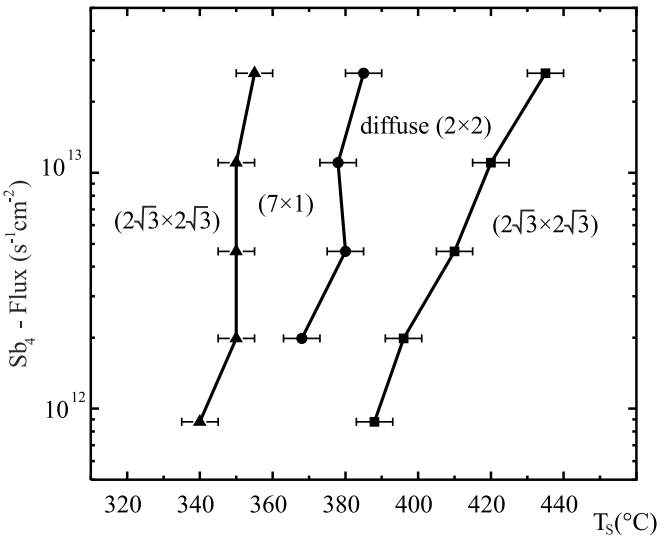

FIG. 9. Surface reconstruction phase diagram for the AlSb(111)*A* surface as a function of Sb_4 flux and substrate temperature.

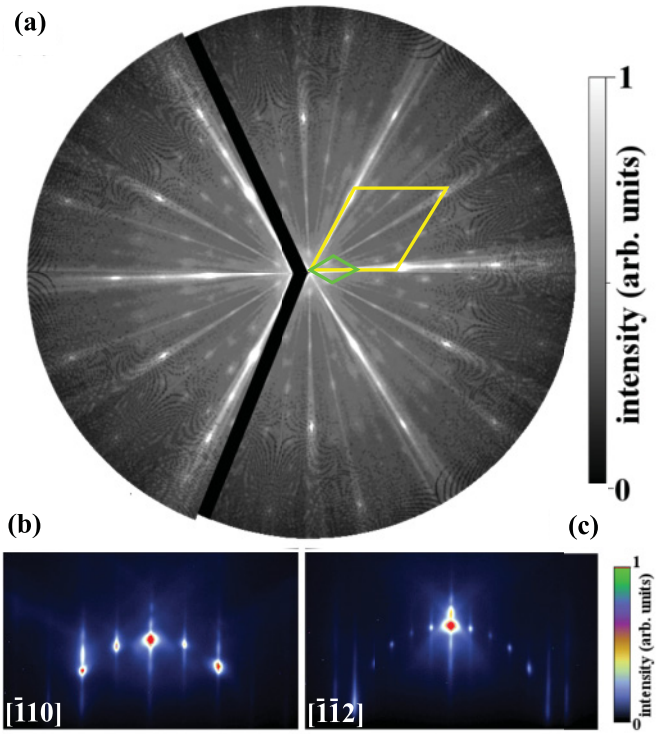

FIG. 10. (Color online) (a) RHEED azimuthal scan of the AlSb(111)A ($2\sqrt{3} \times 2\sqrt{3}$) reconstruction at 320 °C substrate temperature. The big rhombus marks the (1 × 1) surface unit cell and the small rhombus marks the unit cell of the ($2\sqrt{3} \times 2\sqrt{3}$) reconstruction. RHEED pattern recorded with the primary beam along (b) [$\bar{1}$10] and (c) [$\bar{1}\bar{1}$2] incident directions.

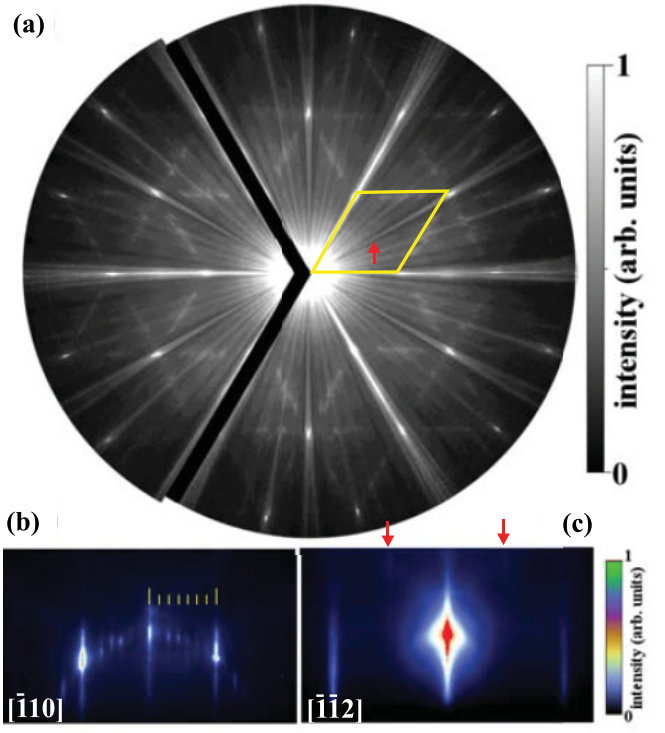

FIG. 11. (Color online) (a) RHEED azimuthal scan of the AlSb(111)A (7 × 1) reconstruction at 350 °C substrate temperature. The rhombus indicates the (1 × 1) surface unit cell and the arrow shows the 2 × periodicity in the [$\bar{1}\bar{1}$2] direction resulting from the rotated domains. RHEED patterns along (b) [$\bar{1}$10] and (c) [$\bar{1}\bar{1}$2] incident directions.

In contrast to the GaSb(111)A ($2\sqrt{3} \times 2\sqrt{3}$) reconstruction, the low-temperature AlSb(111)A ($2\sqrt{3} \times 2\sqrt{3}$) reconstruction does not show stronger 2 × reflections. There are no significant fractional-order intensities at the ($3h$/6,0) position along the [$\bar{1}\bar{1}$2] [Fig. 10(c)] incident direction and their symmetry-equivalent directions. The azimuthal scan reveals a high background level, which is an indication for surface disorder at these low temperatures.

For the AlSb(111)A (7 × 1) reconstruction, the fractional-order rods along the [$\bar{1}$10] incident direction [Fig. 11(b)] are marked by short lines. A measurement of their positions confirms that all rods have the exact 7 × period. There is no disorder or superperiod like in the GaSb(111)A (12×1) reconstruction. Just as on the GaSb(111) surfaces, the 2 × periodicity along the [$\bar{1}\bar{1}$2] incident direction originates from the 120°-rotated diffraction pattern of the (7 × 1) reconstruction and is labeled with an arrow in Fig. 11(a).

Figure 12 presents the diffuse (2 × 1) reconstruction. The scans were measured at 400 °C substrate temperature. The transition temperature from the diffuse (2 × 1) to the high-temperature ($2\sqrt{3} \times 2\sqrt{3}$) reconstruction ranges from 380 to 450 °C depending on the Sb_4 flux. Compared to the low-temperature ($2\sqrt{3} \times 2\sqrt{3}$) reconstruction, the signal-to-noise ratio is higher. The high-temperature $2\sqrt{3}$ reconstruction is more ordered then the low-temperature $2\sqrt{3}$ reconstruction. To confirm our conclusions, a detailed real-space structure analysis would be appropriate by *in situ* x-ray surface diffraction or STM/AFM measurements.

Similar to the GaSb(111)A ($2\sqrt{3} \times 2\sqrt{3}$) reconstruction, a bright fractional-order rod with superimposed intensities at ($3h$/6, 0) is visible along the [$\bar{1}$10] incident direction in Fig. 13(c) for the high-temperature AlSb(111)A ($2\sqrt{3} \times 2\sqrt{3}$) reconstruction. A (2 × 2) reconstruction could also be present besides the high-temperature ($2\sqrt{3} \times 2\sqrt{3}$) reconstruction. While ramping the substrate temperature with a rate of 0.1 K/s, the ($2\sqrt{3} \times 2\sqrt{3}$) reconstruction changes to a (1 × 1) reconstruction at a substrate temperature of around 480 °C, similar to the GaSb(111)A and B surfaces.

The AlSb(111)B surface only has a single (2 × 2) reconstruction in the accessible range of MBE substrate temperatures and Sb_4 fluxes. Without a quantitative analysis by RHEED, it is difficult to distinguish between a (2 × 2) and a (2 × 1) reconstruction with rotated domains. The diffraction peaks of both reconstructions are superimposed. Only the peak intensities and/or shapes of the peaks may differ for these reconstructions. For the AlSb(111)B (2 × 2), the peak intensities measured with RHEED are similar in the three azimuths, and we can therefore assume a (2 × 2) reconstruction. In addition, weak streaks with a 4 × periodicity are observed in the RHEED pattern measured with the beam along the [$\bar{1}\bar{1}$2] incident direction [Fig. 14(c)]. A (4 × 2) reconstruction does not agree with the measured ARHEED scan. The apparent 4 × periodicity results from the shoulders

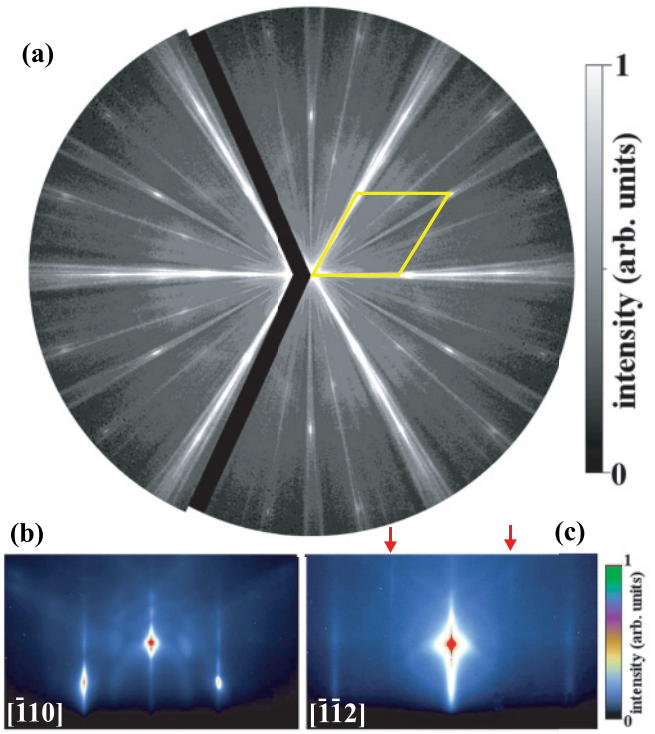

FIG. 12. (Color online) (a) RHEED azimuthal scan of an AlSb(111)*A* diffuse (2×1) reconstruction at 400 °C substrate temperature. The rhombus corresponds to the (1×1) surface unit cell. RHEED patterns along the (b) [$\bar{1}$10] and (c) [$\bar{1}\bar{1}$2] incident directions.

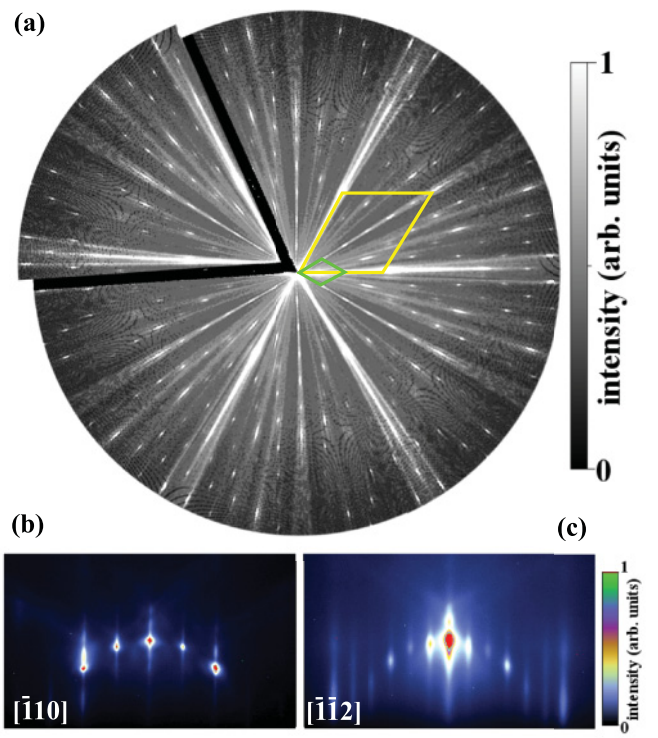

FIG. 13. (Color online) (a) RHEED azimuthal scan of an AlSb(111)*A* $(2\sqrt{3} \times 2\sqrt{3})$ reconstruction at 450 °C substrate temperature. The big rhombus marks the (1×1) surface unit cell and the small rhombus marks the $(2\sqrt{3} \times 2\sqrt{3})$ unit cell. RHEED patterns along (b) [$\bar{1}$10] and (c) [$\bar{1}\bar{1}$2] incident directions.

of (2×2) peak intensities and is observed from room temperature up to 480 °C substrate temperature, where the RHEED pattern changes to the (1×1) symmetry. Changes in the Sb_4 flux do not affect the (2×2) diffraction pattern. Due to oxidation of AlSb, we are not able to investigate the surface morphology of the grown layers by *ex situ* methods like AFM and/or SEM.

C. Structure model building principles

In this section, we consider reconstructions based on our experimental results by applying the electron counting rule (ECR),[65] which is obeyed by the vast majority of stable III-V semiconductor surfaces with a few exceptions, such as GaN.[66] To fulfill the ECR, dangling bonds of group V atoms at the surface are filled with electrons since their energetic position is typically below the Fermi energy close to the top of the bulk valence-band maximum. In contrast, the group III dangling bonds have to be empty since they are energetically above the Fermi energy. Therefore, the resulting surface band structure would be semiconducting when fulfilling the ECR. The surface energy is influenced by the necessary charge transfer, which leads to changes in the electrostatic interactions and the strain introduced due to rebonding of the atoms at the surface. The stable reconstructions on both orientations of (111) III-V semiconductor surfaces fulfill the ECR, with a few exceptions like GaN.[66] They share a common set of structural motifs from which the reconstructions are built.[67] On the basis of the experimentally observed symmetries, one can construct models of possible surface structures combining these structural motifs under the ECR constraint. This will be carried out in the following. These considerations are also transferable to other (111)*A* and (111)*B* surfaces.

Table I lists structural motifs of known stable reconstructions found on (111)*A* surfaces.[67] They differ in the size s_i expressed in the number of the occupied (1×1) surface unit cells and the number of excess electrons l_i to fulfill the ECR. As an example, the standard Ga-terminated (1×1) cell has a size of one (1×1) unit cell and an ECR excess of 3/4 electrons due to the single Ga dangling bond, which should be empty to satisfy the ECR. Reconstructions can now be characterized by the size $N_x \times N_y$ of their unit cell and the number of occurrences n_i $(i = a, \ldots, e)$ of the motifs (see Fig. 15). With this, two constraints can be derived. The first one is defined by the fact that the total number of occupied (1×1) cells, i.e., the sum over the products of motif occurrence n_i and size s_i, has to be identical to the surface unit cell size,

$$\sum_i n_i s_i = N_x \times N_y. \tag{1}$$

Second, to fulfill the ECR, the sum over all excess electrons needs to be zero,

$$\sum_i n_i l_i = 0. \tag{2}$$

Using explicitly the values from Table I for s_i and l_i and substituting n_a in the first equation, one finds that $4\,(n_b + n_c + n_d) =$

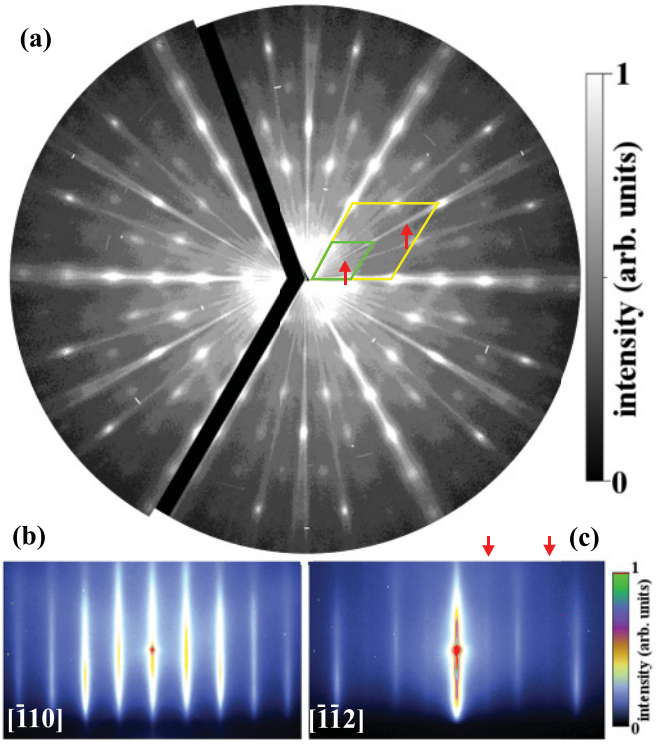

FIG. 14. (Color online) (a) RHEED azimuthal scan of an AlSb(111)B (2 × 2) reconstruction at 300 °C substrate temperature. The big rhombus marks the (1 × 1) surface unit cell and the small rhombus the (2 × 2) unit cell. Two arrows shows the 4 × periodicity along the [$\bar{1}\bar{1}$2] incident direction resulting from the shoulders of the (2 × 2) spots. RHEED patterns along (b) [$\bar{1}$10] and (c) [$\bar{1}\bar{1}$2] incident directions.

$N_x \times N_y$. Since only positive integer numbers are allowed, only unit cells with a size of a multiple of four (1 × 1) unit cells can fulfill this requirement. All observed reconstructions are compatible with this rule, with one exception: the (7 × 1) reconstruction observed on the AlSb(111)A surface. A possible explanation could be disorder due to unit-cell shifts, which hide the full symmetry of the unit cell. Furthermore, the above analysis allows the determination of possible motif combinations, e.g., as input for first-principles calculations. For instance, it follows also from the above equation that at least one of n_b, n_c, or n_d needs to be greater than zero. In other words, every unit cell, to fulfill electron counting, contains either a group V adatom, a group V trimer, or a group III vacancy. It is straightforward to derive further requirements for the combination of the motifs.

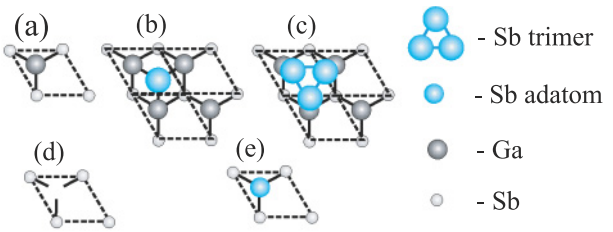

FIG. 15. (Color online) ECR motifs for (111)A surfaces.

TABLE I. Structural motifs of the (111)A surface, their sizes s_i, and their excess electrons according to the ECR (see Fig. 15).

Label i	Description	Size s_i (1 × 1) cells	ECR l_i
(a)	1 × 1 (ideal)	1	3/4
(b)	Group V adatom	3	−3/4
(c)	Group V trimer	3	−3/4
(d)	Group III vacancy	1	−9/4
(e)	Group III-V exchange	1	3/4

In a similar way as for the (111)A surface, the corresponding structural motifs as well as their size and excess electrons for the (111)B surface are listed in Table II. By analogy, we get $4\,(n_b + n_c + n_d + n_e) = N_x \times N_y$ since everything is identical with the exception of the sign and the additional motif (e), which in its properties is identical to (c). The conclusions drawn for the (111)A surface, therefore, apply here as well. All observed symmetries on (111)B reconstructions fulfill this requirement.

IV. SUMMARY

We have investigated the stability ranges and surface symmetries of GaSb and AlSb (111)A and (111)B surface reconstructions prepared by MBE. To this end, planar cuts through reciprocal space parallel to the surface were performed *in situ* by azimuthal scan RHEED (ARHEED). Under different Sb_4 fluxes, we observed two GaSb(111)A, one GaSb(111)B, four AlSb(111)A, and one AlSb(111)B reconstruction as a function of substrate temperature.

The stationary RHEED and ARHEED scans of the GaSb and AlSb(111) surfaces demonstrate that all reconstructions have a threefold symmetry. The GaSb(111)A (12 × 1), GaSb(111)B (8 × 1), AlSb(111)A (7 × 1), and AlSb(111)A (2 × 1) reconstructions consist of three domains. In addition, these reconstructions may contain disordered structure motifs. We have shown that the 2 × periodicity along the [$\bar{1}\bar{1}$2] incident direction corresponds to a projection of diffraction intensity streak shoulders along the [$\bar{1}$10] incident direction. Stationary RHEED alone would not be sufficient to draw this conclusion.

An unambiguous exclusion of the (2 × 2) reconstruction coexisting with the $(2\sqrt{3} \times 2\sqrt{3})$ reconstruction is not possible based on qualitative RHEED measurements. Therefore, additional experiments like STM or *in situ* x-ray diffraction are

TABLE II. Structural motifs of the (111)B surface, their size s_i, and their excess electrons according to the ECR.

Label i	Description	Size s_i (1 × 1) cells	ECR l_i
(a)	1 × 1 (ideal)	1	−3/4
(b)	Group III adatom	3	3/4
(c)	Group III trimer	3	3/4
(d)	Group V vacancy	1	9/4
(e)	Group V trimer	3	3/4
(f)	Group V-III exchange	1	−3/4

required to resolve this open question. The present study has shown that the reported GaSb(111)*A* (5 × 2) reconstruction actually is a (12 × 1) reconstruction. Under Ga-rich conditions, a (2 × 2) on GaSb(111)*A*, a (3 × 3) on GaSb(111)*B*, and a (2 × 2) reconstruction appears on both the AlSb(111)*A* and (111)*B* surfaces. Since significant differences exist in the stable reconstruction symmetries, the results can serve as a basis to determine the (111) surface polarity as well as possible polarity inversions in heteroepitaxial growth.

All observed surface reconstructions are consistent with possible structure models derived by applying the electron counting rule with known motifs with a single exception: the (7 × 1) reconstruction observed on the AlSb(111)*A* surface.

ACKNOWLEDGMENTS

Support by the German Research Foundation (GZ: 436 TSE 113/62/0-1) and the Institutional Research Plan No. AVOZ 10100521 is gratefully acknowledged. We thank Steffen Behnke and Carsten Stemmler for technical support and Oliver Brandt for a careful reading of the manuscript.

*proessdorf@pdi-berlin.de

[1] S. Ino, Jpn. J. Appl. Phys. **16**, 891 (1977).
[2] W. Braun, H. Möller, and Y. H. Zhang, J. Vac. Sci. Technol. B **16**, 1507 (1998).
[3] W. Braun, H. Möller, and Y. H. Zhang, J. Vac. Sci. Technol. B **17**, 474 (1998).
[4] A. Ichimiya and P. I. Cohen, *Reflection High-Energy Electron Diffraction* (Cambridge University Press, 2011), p. 366.
[5] R. Feidenhans'l, Surf. Sci. Rep. **10**, 105 (1989).
[6] K. W. Haberern and M. D. Pashley, Phys. Rev. B **41**, 3226 (1990).
[7] W. Barvosa-Carter, R. S. Ross, C. Ratsch, F. Grosse, J. H. G. Owen, and J. J. Zinck, Surf. Sci. Lett. **499**, L129 (2002).
[8] J. W. Kim, S. Kim, J. M. Seo, S. I. Tanaka, and M. Kamada, Phys. Rev. B **54**, 4476 (1996).
[9] J. M. C. Thornton, P. Weightman, D. A. Woolf, and C. J. Dunscombe, Phys. Rev. B **51**, 14459 (1995).
[10] J. J. Zinck, R. S. Ross, J. H. G. Owen, W. Barvosa-Carter, F. Grosse, and C. Ratsch, Appl. Phys. Lett. **79**, 2354 (2001).
[11] T. Nakada and T. Osaka, Phys. Rev. Lett. **67**, 2834 (1991).
[12] W. G. Schmidt, Appl. Phys. A **75**, 89 (2002).
[13] W. Barvosa-Carter, A. S. Bracker, J. C. Culbertson, B. Z. Nosho, B. V. Shanabrook, L. J. Whitman, H. Kim, N. A. Modine, and E. Kaxiras, Phys. Rev. Lett. **84**, 4649 (2000).
[14] M. C. Righi, R. Magri, and C. M. Bertoni, Phys. Rev. B **71**, 075323 (2005).
[15] B. P. Tinkham, O. Romanyuk, W. Braun, K. H. Ploog, F. Grosse, T. Takahasi, T. Kaizu, and J. Mizuki, J. Electron. Mater. **37**, 1793 (2008).
[16] O. Romanyuk, W. Braun, and F. Grosse, e-J. Surf. Sci. Nanotech. **7**, 429 (2009).
[17] O. Romanyuk, F. Grosse, and W. Braun, Phys. Rev. B **79**, 235330 (2009).
[18] P. M. Thibado, B. R. Bennett, B. V. Shanabrook, and L. J. Whitman, J. Cryst. Growth **175**, 317 (1997).
[19] A. S. Bracker, M. J. Yang, B. R. Bennett, J. C. Culbertson, and W. J. Moore, J. Cryst. Growth **220**, 384 (1991).
[20] F. Grosse, W. Barvosa-Carter, J. Zinck, M. Wheeler, and M. F. Gyure, Phys. Rev. Lett. **89**, 116102 (2002).
[21] O. Yilmazoglu, M. Brandt, J. Sigmund, E. Genc, and H. L. Hartnagel, Sens. Actuators A **94**, 59 (2001).
[22] H. Yasuda and I. Hosako, Jpn. J. Appl. Phys **47**, 1575 (2008).
[23] T. J. Rotter *et al.*, Appl. Phys. Express **2**, 112102 (2009).
[24] A. Olivier *et al.*, IPRM 2008, 20th International Conference on Indium Phosphide and Related Materials (2008), Vol. 1, p. 1.
[25] M. Grau, C. Lin, O. Dier, C. Lauer, and M.-C. Amann, Appl. Phys. Lett. **87**, 241104 (2005).
[26] L. Shterengas, G. Belenky, M. V. Kisin, and D. Donetsky, Appl. Phys. Lett. **90**, 011119 (2007).
[27] H. Kroemer, J. Cryst. Growth **81**, 193 (1987).
[28] D. Cohen and C. B. Carter, J. Microsc. **208**, 84 (2002).
[29] T. Watahiki, F. Grosse, W. Braun, V. M. Kaganer, A. Proessdorf, A. Trampert, and H. Riechert, Appl. Phys. Lett. **97**, 1 (2010).
[30] S. C. Lee, L. R. Dawson, S. R. J. Brueck, and Y.-B. Jiang, Appl. Phys. Lett. **87**, 023101 (2005).
[31] H. Lipson and K. E. Singer, Surf. Sci. **4**, 247 (1966).
[32] G. J. Russell, Surf. Sci. **55**, 380 (1976).
[33] A. J. van Bommel and J. E. Crombeen, Surf. Sci. **93**, 383 (1980).
[34] R. Feidenhans'l, M. Nielsen, R. J. F. Grey, and I. Robinson, Surf. Sci. **186**, 499 (1987).
[35] A. Belzner, E. Ritter, and H. Schulz, Surf. Sci. **209**, 379 (1989).
[36] T. van Gemmeren and R. L. Johnson, Condens. Matter **9**, 4603 (1997).
[37] J. L. Guyaux, R. Sporken, R. Caudano, V. Wagner, J. Geurts, N. Esser, and W. Richter, Surf. Sci. **338**, 204 (1995).
[38] O. Romanyuk, F. Grosse, A. Proessdorf, W. Braun, and H. Riechert, Phys. Rev. B **82**, 125315 (2010).
[39] G. P. Schwartz, G. J. Gualtieri, and W. A. Sunder, J. Cryst. Growth **102**, 147 (1990).
[40] J. A. Dura, J. T. Zborowski, and T. D. Golding, in *Molecular Beam Epitaxy Study of InAs/GaSb Heteroepitaxy on the (111)A and (111)B Orientations*, Materials Research Society Symposium Proceedings No. 263 (MRS, Pittsburgh, 1992), p. 35.
[41] J. A. Dura, A. Vigliante, T. D. Golding, and S. C. Moss, J. Appl. Phys. **77**, 21 (1995).
[42] T. Shibata, J. Nakata, Y. Nanishi, and M. Fujimoto, Jpn. J. Appl. Phys. **33**, 1767 (1994).
[43] B. Jenichen, W. Braun, V. M. Kaganer, A. G. Shtukenberg, L. Däweritz, C.-G. Schulz, K. H. Ploog, and A. Erko, Rev. Sci. Instrum. **74**, 1267 (2003).
[44] V. T. S. Schwarz, SAFIRE, FhG Erlangen (2008).
[45] R. J. Bennett and C. Parish, J. Phys. D **9**, 2555 (1976).
[46] T. Abukawa, T. Yamazaki, K. Yajima, and K. Yoshimura, Phys. Rev. Lett. **97**, 245502 (2006).
[47] O. Romanyuk, K. Kataoka, F. Matsui, K. Hattori, and H. Daimon, Czech. J. Phys. **56**, 267 (2006).
[48] H. Yamaguchi and Y. Horikoshi, Phys. Rev. Lett. **70**, 1299 (1993).
[49] H. Yamaguchi and Y. Horikoshi, Phys. Rev. B **48**, 2807 (1993).
[50] T. Kita, M. Nakamoto, and O. Wada, Phys. Rev. B **67**, 193306 (2003).

[51]O. Romanyuk, F. Grosse, and W. Braun, Phys. Status Solidi C **7**, 330 (2010).

[52]See supplemental material at [http://link.aps.org/supplemental/10.1103/PhysRevB.83.155317] for a RHEED pattern of the GaSb(111)*A* (12×1) reconstruction comparing low- and high-resolution RHEED images.

[53]K. Hermann, LEEDPat22, Fritz-Haber Institut der MPG (2010).

[54]M. Nishizawa, T. Eguchi, T. Misima, J. Nakamura, and T. Osaka, Phys. Rev. B **57**, 6317 (1998).

[55]Y. H. Kim, J. Y. Lee, Y. G. Noh, M. D. Kim, S. M. Cho, Y. J. Kwon, and J. E. Oh, Appl. Phys. Lett. **88**, 241907 (2006).

[56]J. Tatebayashi, A. Jallipalli, M. N. Kutty, S. Huang, K. Nunna, G. Balakrishnan, L. R. Dawson, and D. L. Huffaker, IEEE J. Sel. Top. Quantum Electron. **15**, 716 (2010).

[57]H. S. Kim, Y. K. Noh, M. D. Kim, Y. J. Kwon, J. E. Oh, Y. H. Kim, J. Lee, S. Kim, and K. S. Chung, J. Cryst. Growth **301**, 230 (2007).

[58]C. Ratsch, Phys. Rev. B **63**, 161306 (2001).

[59]W. Martienssen and H. Warlimont, *Springer Handbook of Condensed Matter and Materials Data*, 1st ed. Vol. 1. (Springer, Berlin, 2005).

[60]M. Gonzalez-Debs, J. G. Cederberg, R. M. Biefeld, and T. F. Kuecha, J. Appl. Phys. **97**, 103522 (2005).

[61]A. M. Dabiran and P. I. Cohen, J. Cryst. Growth **150**, 23 (1995).

[62]J. Harper, M. Weimer, D. Zhang, C.-H. Lin, and S. S. Pei, J. Vac. Sci. Technol. B **16**, 3 (1998).

[63]J. Harper, M. Weimer, D. Zhang, C.-H. Lin, and S. S. Pei, Appl. Phys. Lett. **73**, 2805 (1998).

[64]G. J. Sullivan, A. Ikhlassi, J. Bergman, R. E. DeWames, J. R. Waldrop, C. Grein, K. Mahalingam, H. Yang, M. Zhong, and M. Weimer, J. Vac. Sci. Technol. B **23**, 1144 (2005).

[65]M. D. Pashley, Phys. Rev. B **40**, 10481 (1989).

[66]A. R. Smith, R. M. Feenstra, D. W. Greve, M. S. Shin, M. Skowronski, J. Neugebauer, and J. E. Northrup, J. Vac. Sci. Technol. B **16**, 2242 (1998).

[67]N. Moll, A. Kley, E. Pehlke, and M. Scheffler, Phys. Rev. B **54**, 8844 (1996).